

Hot gas haloes around disc galaxies: O VII column densities from galaxy formation simulations

E. Ntormousi^{1,2*} and J. Sommer-Larsen^{3,4,5}

¹*Universitäts-Sternwarte, Munich D-81679, Germany*

²*Max-Planck Institut für Extraterrestrische Physik, 85741 Garching Germany*

³*Dark Cosmology Center, Niels Bohr Institute, University of Copenhagen, Juliane Maries Vej 30, DK-2100 Copenhagen, Denmark*

⁴*Excellence Cluster Universe, Boltzmannstr. 2 85748 Garching, Germany*

⁵*Marie Kruses Skole, Stavnsholtvej 29-31, DK-3520 Farum, Denmark*

Accepted 2010 July 13. Received 2010 July 2; in original form 2010 April 9

ABSTRACT

Numerical models of disc galaxy formation predict the existence of extended, hot ($T \sim 10^6$ K) gas haloes around present day spirals. The X-ray luminosity of these haloes is predicted to increase strongly with galaxy mass. However, searches for their X-ray emission have not been successful so far.

We calculate the all sky O VII column density distributions for the haloes of three Milky Way like disc galaxies, resulting from cosmological high-resolution, N-body/gasdynamical simulations. We perform calculations both including the disc gas and without it, so the disc contribution to the column density is quantified. It is found that the column densities estimated for Milky Way-like galaxies are just below the observational upper limit, making a test of the hot halo paradigm likely within observational reach.

Key words: galaxies: formation – galaxies:haloes – galaxies:spiral – X-rays: galaxies.

1 INTRODUCTION

Numerical simulations of disc galaxy formation predict that disc galaxies, not only in groups or clusters, but also in isolation, should reside in extended, hot gaseous haloes ($T \sim 10^6$ K). This gas is accreted from the intergalactic medium and cools out as it settles onto the disc, thus contributing to the formation of the galaxy. The mass of the predicted halo gas is comparable to the total baryonic mass of the galactic disc and could be the answer to the ‘missing galactic baryons’ problem (Sommer-Larsen 2006).

Gas at temperatures $T \sim 10^6$ K is best studied in the X-ray regime. The X-ray luminosities of the galactic haloes are predicted to depend strongly on the characteristic circular velocity of the galaxy, $L_X \propto V_c^7$ (Toft et al. 2002) and should be detectable for the most massive galaxies. However, searches for this X-ray emitting gas have so far been unsuccessful for quiescent disc galaxies. Given the $L_X \propto V_c^7$ scaling, the most restrictive test has been performed by Rasmussen et al. (2009), who observed the halo of the $V_c = 307$ km/s, quiescent, edge-on disc galaxy NGC 5746,

and obtained an upper limit compatible with, but not far from, theoretical predictions.

Plenty of evidence of a hot dilute halo around the Milky Way exists at present: 1) the head-tail structure of many of the high-velocity HI clouds (HVCs) indicates that they are moving in a medium much more hot and dilute than themselves (Brüns et al. 2000; Ganguly et al. 2005), 2) the absence of HI in Local Group dwarf galaxies within ~ 270 kpc distance of either the Milky Way or M31 (Grcevich & Putman 2009), 3) the Magellanic Stream (Stanimirović et al. 2008), given the revised orbit of the LMC (Mastropietro 2009) and 4) high-velocity O VI line absorption in quasar spectra (Sembach et al. 2003; Wakker et al. 2005). O VI probes gas at temperatures near 10^5 K, so high-velocity O VI associated with hydrogen indicates a thermally unstable interface between the high velocity cool clouds and a hot surrounding medium. Moreover, cool-out of hot halo gas, at a rate of $\sim 1 M_\odot/\text{yr}$ is indicated by SiIII absorption by high- and intermediate-velocity clouds in the spectra of AGNs (Shull et al. 2009). Finally, the warm-hot phase of the intergalactic medium (Nicastro et al. 2005) provides a reservoir of hot and dilute gas at galactic distances.

Six times ionized oxygen is indicative of temperatures around 10^6 K so, considering the high cosmic oxygen abun-

* E-mail: eva@usm.uni-muenchen.de (EN); jslarsen@astro.ku.dk (JSL)

Table 1. Numerical and physical characteristics of the galaxy simulations at $z=0$: mass of DM/(high-res)gas/star particles and the respective gravitational (spline) softening lengths; total number of particles, total number of SPH particles and total number of SPH particles after removal of disc etc.; virial mass and radius of the galaxy halo; characteristic circular speed of the galaxy

run	m_{DM}	m_{gas} [$10^6 M_{\odot}/h$]	m_*	ϵ_{DM}	ϵ_{gas} [kpc/h]	ϵ_*	N_{tot}	N_{SPH}	N'_{SPH}	M_{vir} [$10^{12} M_{\odot}$]	R_{vir} [kpc]	V_c [km/s]
K33	0.52	0.093	0.093	0.34	0.19	0.19	1120000	291000	227000	0.39	196	180
K26	4.2	0.012	0.73	0.68	0.095	0.38	733000	534000	333000	0.61	230	207
K15	4.2	0.012	0.73	0.68	0.095	0.38	780000	552000	458000	0.90	262	245
K33LR	4.2	0.012	0.73	0.68	0.095	0.38	537000	425000	257000	0.39	196	180

dance, the O VII line is the best way to check for the existence of a hot gas halo around the Milky Way on the basis of absorption line studies. Absorption in X-rays has been routinely observed at zero redshift for some time (Nicastro et al. 2002; Rasmussen et al. 2003; Fang et al. 2006), but the question of where exactly this gas is located remains under study. Bregman & Lloyd-Davies (2007) compared X-ray absorption between lines of sight in different directions on the sky, and concluded a galactic halo origin for the absorbing gas is plausible. Yao et al. (2008) made a search for the X-ray halo of the Milky Way by comparing O VII line absorption between spectra of objects at different distances and positions relative to the galactic plane. The difference between absorption in sightlines that mostly probe the disc and others that also probe the halo provides an upper limit on the contribution of the halo gas to the total absorption. From this study, an upper limit of $N(OVII) < 5 \cdot 10^{15} \text{ cm}^{-2}$ was found for the sightline considered through the galactic halo. Yao et al. (2010) calculated a somewhat lower column-density contribution of the putative galactic haloes to X-ray absorption by stacking observations towards AGNs and using the intervening galaxies as tracers. Their study gave an upper limit to the ionic column densities coming from galaxy haloes ranging from $\log(N(OVII)) < 14.2-14.8$, but we note that these constraints are less restrictive, since the sight-lines will, in general, pass through the haloes at considerable distances from the galaxy centres - see also the discussion in section 4.

In this paper we show that there is no discrepancy between these observational limits and predictions from galaxy formation simulations. Given information on gas density, temperature, oxygen abundance and UVB radiation field from the simulations, we use the (photo-)ionization code CLOUDY (Ferland et al. 1998) to determine the O VII column density along all lines-of-sight (from positions in the disc corresponding to the location of the sun in the Galactic disc) in the simulated galaxies. We perform the analysis with and without the contribution from the disc gas included.

The structure of this paper is as follows: In section 2 we describe the method we used for our calculations, in section 3 we present the results, and in section 4 we discuss the results obtained.

2 NUMERICAL METHOD

2.1 The N-body/gasdynamical galaxy formation simulations

For our analysis we used three simulated, Milky Way like disc galaxies, resulting from cosmological galaxy formation and evolution simulations based on a flat Λ CDM cosmology ($\Omega_m = 0.3, \Omega_{\Lambda} = 0.7$).

The code used for the simulations was a significantly improved version of the TreeSPH code, which has been used previously for galaxy formation simulations (Sommer-Larsen et al. (2003), in the following SLGP). The main improvements over the previous version are: (1) The “conservative” entropy equation solving scheme suggested by Springel & Hernquist (2002) has been adopted. (2) Non-instantaneous gas recycling and chemical evolution, tracing 10 elements (H, He, C, N, O, Mg, Si, S, Ca and Fe), has been incorporated in the code following Lia et al. (2002a,b); the algorithm includes supernovae of type II and type Ia, and mass loss from stars of all masses. (3) Atomic radiative cooling depending both on the metal abundance of the gas and on the meta-galactic UV field, modelled after Haardt & Madau (1996) is invoked, as well as simplified treatment of radiative transfer, switching off the UV field where the gas becomes optically thick to Lyman limit photons on scales of ~ 1 kpc.

Simulations of three disc galaxies, of mass and size comparable to that of the Milky Way, were used for the present work. The galaxies selected, denoted K33, K26 and K15 in the following, represent “field” galaxies (SLGP), and have, at $z=0$, characteristic circular speeds of $V_c = 180, 207$ and 245 km/s, and virial masses of $0.4-0.9 \times 10^{12} M_{\odot}$.

The galaxies (galaxy DM haloes) were initially selected from a cosmological, DM-only simulation of box-length $10 h^{-1}$ Mpc (comoving), and starting redshift $z_i=39$. Mass and force resolution was increased in Lagrangian regions enclosing the galaxies, and in these regions all DM particles were split into a DM particle and a gas (SPH) particle according to an adopted universal baryon fraction of $f_b=0.15$, in line with recent estimates. Particle numbers for the three TreeSPH simulations were in the range $0.3-1.1 \times 10^6$ (comparison to a lower resolution simulation consisting of 1.5×10^5 particles will be briefly made).

For the galaxy of $V_c = 180$ km/s, $m_{gas}=m_*=9.3 \times 10^4$ and $m_{DM}=5.2 \times 10^5 h^{-1} M_{\odot}$. Moreover, gravitational (spline) softening lengths of $\epsilon_{gas}=\epsilon_*=190$ and $\epsilon_{DM}=340 h^{-1}$ pc, respectively, were adopted. For the galaxies of $V_c = 207$ and 245 km/s, $m_{gas}=m_*=7.3 \times 10^5$ and $m_{DM}=4.2 \times 10^6 h^{-1} M_{\odot}$, and $\epsilon_{gas}=\epsilon_*=380$ and $\epsilon_{DM}=680 h^{-1}$ pc. The gravity (spline)

softening lengths were fixed in physical coordinates from $z=6$ to $z=0$, and in comoving coordinates at earlier times.

A Kroupa IMF was used in the simulations, and early rapid and self-propagating star-formation (sometimes dubbed “positive feedback”) was invoked (SLGP). Finally, in order to enable some reuse of previous work, values of $h=0.65$ and $\sigma_8=1.0$ were employed in the cosmological simulations. Test simulations adopting $h = 0.7$ and $\sigma_8 = 0.9$ give very similar results, since they produce in total only about 5 – 10% more hot gas (Sommer-Larsen 2006).

In order to increase the resolution of the (dilute) halo gas, and enable the formation of a halo multi-phase medium (though still dominated by the hot gas phase; Sommer-Larsen 2006), for galaxies K15 and K26 (which were run at eight times lower mass resolution and two times lower force resolution than K33), each gas particle of $T > 20000$ K, was split into 8 particles 0.7 Gyr before the end of the simulation (i.e., $z=0$). The simulations were then continued for 0.2 Gyr, and, for galaxies K26 and K33, each gas particle of $T > 20000$ K was then again split into 8 gas particles. The resulting ultra-high resolution gas particle mass was $1.2 \times 10^4 h^{-1} M_\odot$, and gravity softening length $\epsilon_{\text{gas}} = 95 h^{-1} \text{pc}$ for the two simulations, which were then continued for an additional 0.5 Gyr, till $z=0$. This allows the development of a multi-phase halo gas structure, including neutral gas clouds (“high-velocity clouds”) — more detail is given in Sommer-Larsen (2006) and Peek et al. (2008).

Finally, to test for effects of numerical resolution, a simulation of galaxy K33, but at the (lower) resolution of galaxies K26 and K15, was also run. Moreover, as detailed above, gas particles of $T > 20000$ K were split into 8 particles 0.7 Gyr before the end of the simulation and yet again split into 8 particles 0.5 Gyr before $z=0$.

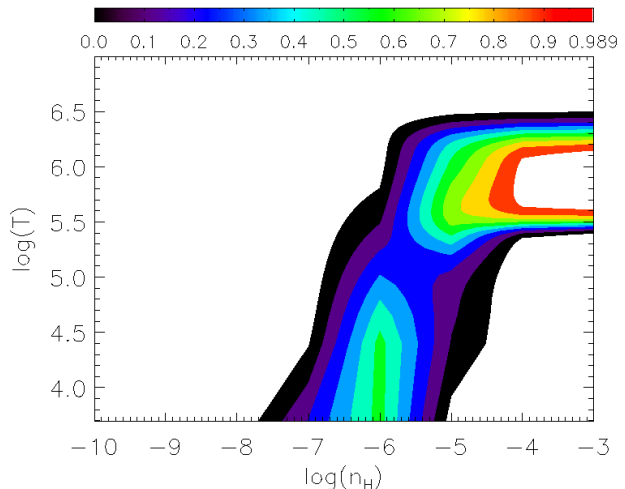
2.2 Oxygen fractions from CLOUDY

We calculated the fraction of oxygen in each ionisation state using CLOUDY version 7.2, last described by Ferland et al. (1998). CLOUDY is a spectral synthesis code, designed to simulate astronomical plasmas.

We used the code for a plane-parallel geometry setup, assuming constant temperature of the gas and including a background UV ionizing field from Haardt & Madau (1997), adapted to $z = 0$ as described in CLOUDY’s user guide. The calculation was done for a single zone and iteration was allowed to continue until convergence. We thus created a look-up table of O VII fractions for hydrogen densities ranging from $\log n_H = -10$ to $\log n_H = -3$ and gas temperatures from $\log T = 3.5$ to $\log T = 7$. The gas was assumed to be optically thin to the UV radiation. Self shielding of the cold and dense gas was approximated by “turning off” the UV background for temperatures $T < 20000$ K and densities $n_H > 10^{-3} \text{cm}^{-3}$ — this condition, at $z \sim 0$, effectively mimics the (simplified) UVB radiative transfer invoked in the galaxy formation simulations.

Without a background radiation field and for thermodynamical equilibrium, ionisation fractions only depend on the gas temperature, according to the Saha equation (Saha 1921). However, with the inclusion of the UV field, the ionization state also depends on the density. The dependence of the O VII fraction on density and temperature, at $z=0$, is shown in Figure 1.

Figure 1. O VII fractions, f_7 , calculated using CLOUDY and invoking a $z=0$ Haardt & Madau background UV field. The effect of the UV field becomes significant at hydrogen densities $n_H \lesssim 10^{-4} \text{cm}^{-3}$



2.3 Calculating O VII column densities

For our analysis we used SPH simulation data for three spiral galaxies. We calculated column densities as,

$$N(OVII) = \sum^N n_{OVII} \cdot d, \quad (1)$$

with

$$n_{OVII} = n_H \cdot Z_{O,sim} \cdot Z_{O,\odot} \cdot f_7, \quad (2)$$

where n_H is the hydrogen number density in cm^{-3} , $Z_{O,sim}$ is the oxygen abundance in units of solar, $Z_{O,\odot}$ is the solar oxygen number abundance from Asplund et al. (2005), d the distance in cm between two points on a line of sight, f_7 is the fraction of oxygen in the sixth ionisation state and the sum is over a set of equidistant points along a given line of sight. n_H and $Z_{O,sim}$ were given by the simulations, while the oxygen fractions were calculated using CLOUDY, as described in section 2.2.

For each of the simulated galaxies we drew lines of sight from within the disc into the halo, covering all the sky. The starting point of each line was placed on the midplane of the disc, approximately 8 kpc from the centre and the integration was carried into the halo, up to a distance of 500kpc. The choice of 500kpc is discussed in section 3.

Each line of sight was represented by 150 equidistant points and to each point \vec{p} , a smoothing length was assigned,

$$h_{\vec{p}} = \frac{1}{4}(d_{50} + d_{51}), \quad (3)$$

where $h_{\vec{p}}$ is the smoothing length of the line point and d_{50} and d_{51} are the distances of the 50th and 51st closest SPH particles to the point, respectively. This choice was made for consistence with the SPH calculations, which use the 50 closest neighbours of a particle to evaluate interaction forces. All quantities of interest were then averaged over a sphere of radius $2h_{\vec{p}}$, centred on the point \vec{p} , using a cubic spline

weighting function that mimics the SPH kernel function, and attributed to the point.

Specifically, for each SPH particle, on the basis of the density and temperature, the OVII fraction, f_7 , was calculated using the CLOUDY based lookup table we have created. Using the oxygen abundance, n_{OVII} was then determined. These values were then interpolated onto the individual line-of-sight points, as described above. Finally, eq.1 was used to calculate $N(OVII)$ along a given line-of-sight.

For choosing the number of points to represent a line of sight, we compared the results of 20000 line of sight calculations, each done using 150 points and then repeated using 500 points and found only insignificant differences in the column densities. Higher line-of-sight resolution than this is not justified, as we would then interpolate particle properties over distances smaller than the SPH smoothing lengths.

3 RESULTS

Not only hot halo gas may contribute to the O VII column density along a given line-of-sight. Also gas in the disc, heated by feedback from super-nova explosions or photo-ionized, may contain O VII. Furthermore, satellite galaxies with ongoing star formation and related super-nova feedback, as well as the photo-ionized surface layers of HI clouds in the halo (HVCs), may contribute to the O VII column density along some lines-of-sight.

In our first set of $N(OVII)$ estimates, in order to exclude such “contaminating” gas, we excluded all disc gas within a cylinder of radius $r = R_d = 20$ kpc, where R_d the galactic disc radius and height $z = \pm 3$ kpc, centred at the centre of the galaxy, and aligned with the disc. Moreover, it was found that potentially “contaminating” gas in satellites as well as in halo HI clouds was characterized by densities $n_H > n_{H,c}$, where $n_{H,c} = 10^{-3} \text{ cm}^{-3}$. On the other hand, the hot halo gas was found to everywhere have $n_H < n_{H,c}$. We hence excluded all gas in the halo of $n_H > n_{H,c}$ from the analysis. The filling factor of this gas is very small, $f \ll 0.01$, and the effect of excluding it on the results presented in the following is negligible.

In order to assess the effect of removing the potentially contaminating gas we made a second set of $N(OVII)$ estimates based on all gas, i.e., including gas in the disc, satellite galaxies and HI clouds.

We should note here that, when choosing our lines of sight, as a first approach we did not try to achieve the same resolution in all areas of the celestial sphere. However, any over- or under- sampling of areas could result in differences in the calculated distributions. For this reason, we have compared between a constant 1 degree separation of the lines of sight and a simple weighting scheme that samples each galactic longitude with $360 \cdot \cos b$ lines, where b is the galactic latitude of the line of sight, and found little difference in the statistics. In the following we use the constant resolution for illustration purposes only and present all the analysis for the data calculated with the weighting scheme.

Figure 2 shows the all sky, statistical $N(OVII)$ distributions for the three galaxies and two types of estimates, employing the weighting scheme outlined above and figure 3 shows the cumulative histograms of the calculated column densities.

Figure 4 shows contours of the logarithm of the O VII column density as a function of galactic longitude and latitude when all disc and “dense” (see above) halo gas particles are removed from the simulation data. Figure 5 shows the results with all the particles included. Both results have been calculated with a constant one degree distance between the lines of sight.

For all galaxies, the halo only O VII column density is below the observational upper limit of $\sim 5 \cdot 10^{15} \text{ cm}^{-2}$ (Yao et al. 2008). There is a spread of approximately one order of magnitude in column density values that results from local fluctuations in density and/or metallicity.

With the inclusion of all SPH particles the mean column density is not significantly affected, but the distributions all display a tail towards higher column densities (see Table 2 and figures 2 and 3). The areas near the galactic plane are dominated by disc contribution, while halo objects give extended high column density areas at latitudes away from the galactic plane.

As can be seen from figure 5, high O VII column densities are quite common when the disc is included. This is due to supernova explosions heating the gas and, of course, due to the high metallicity of the disc gas. It is worth noting that a feature near the disc plane of K26 can still be seen in figure 4, when the disc is removed. This is a typical example of the effects of supernova-driven outflow, driving high-metallicity hot gas into the lower halo. In the case of K33, the characteristic features in Figure 5 come from a large warp surrounding the galaxy, product of the tidal disruption of a satellite, previously accreted onto the galaxy.

In order to assess how the inclusion of the cosmic UV background affects the results, we repeated the halo-only run using an oxygen fraction table calculated without a UV background. As illustrated in the left panel of Figure 2, the overall effect of the UV field is to shift the distribution to slightly lower column densities. This happens because the hardest photons of this radiation can ionise oxygen to levels higher than the sixth, so the latter remains relatively underpopulated. However, this is not the case for K33, where the UV background has the opposite effect, that is to increase the column density values. This is easily understood, since the average temperature of the K33 halo is somewhat lower, due to its lower mass, so the UV field brings oxygen from lower ionisation stages to the sixth.

The distance of 500kpc at which we decided to stop the integration was chosen so that we would only probe the halo of a single galaxy. Integrating to a somewhat smaller distance of 300kpc does not affect the results significantly, owing to the low gas densities at these distances from the galaxy. For distances larger than 500kpc, one could consider the possibility that a line of sight passes through the haloes of neighbouring galaxies, which would in principle also give a contribution. To test the effect of a line of sight intersecting the halo of a neighbouring galaxy we calculated the $N(OVII)$ values for 10000 random lines of sight passing through the halo of K15 (this galaxy was chosen because the virial temperature is comparable to that of M31 — see section 4). The lines of sight were chosen to originate and end at $r=500$ kpc distance from the central galaxy. Figure 6 shows the result of this calculation for impact parameters up to 300kpc. For larger impact parameters the contribution drops even further.

Table 2. Mean logarithm of column densities $\langle \log N(OVII) \rangle$ for different runs.

Galaxy	Mean $\log N(OVII)$ without disc	Mean $\log N(OVII)$ including disc	Mean $\log N(OVII)$ without UV or disc
K33	13.55	13.72	13.46
K26	14.13	14.42	14.25
K15	14.41	14.55	14.54

It is apparent from Figure 6 that, unless a line of sight passes through a neighbouring halo with an impact parameter lower than ~ 100 -200kpc, the contribution from this halo will be negligible.

4 DISCUSSION AND CONCLUSIONS

We have in this work determined the O VII column density of hot halo gas along various lines-of-sight in three simulated disc galaxies. In order to emulate observations performed at the solar position in the Milky Way, we have, in each galaxy, chosen a position in the midplane of disc, located 8 kpc from the centre of the galaxy. From this position we have drawn lines-of-sights emulating all sky coverage.

We have tested that the results obtained do not in any significant way depend on where, along the $R = 8$ kpc mid-plane circle, the observer is assumed to be located. Moreover, we have for galaxy K33 tested that the results obtained do not in any significant way depend on the numerical resolution of the galaxy formation simulation.

For the two Milky Way sized galaxies, of $V_c = 207$ and 245 km/sec, respectively, we find median halo gas O VII column densities of 1.5 - $2.5 \cdot 10^{14}$ cm^{-2} , with a dispersion in $\log(N(OVII))$ of about 0.2. For the somewhat smaller disc galaxy K33, of $V_c = 180$ km/s, we find a median halo gas O VII column density of $3 \cdot 10^{13}$ cm^{-2} , also with a dispersion in $\log(N(OVII))$ of about 0.2. The lower value for this galaxy is primarily due to the somewhat lower (virial) temperature of the hot gas (by about a factor of two), which, cf. Fig. 1, leads to a significant reduction of the number of oxygen ions in the sixth ionization stage for the relevant density range, $n_H \sim 10^{-6} - 10^{-3.5}$ cm^{-3} .

The main result of the paper is hence that for the two Milky Way sized galaxies, the median predicted halo O VII column density lies about a factor of 20 below the observational upper limit of $5 \cdot 10^{15}$ cm^{-2} reported by Yao et al. (2008) (and is comparable to the upper limits of $\log(N(OVII)) < 14.2 - 14.8$ set by Yao et al. (2010), but these limits are based on halo sight-lines, in general, passing far away from the galactic centres a comparison is less straightforward — see also below). Moreover, not a single line-of-sight was found in any of the galaxies with a halo O VII column density exceeding the Yao et al. (2008) limit.

When the disc gas, as well as gas in satellites and HI clouds, is not excluded in the O VII column density estimates, the median $N(OVII)$ increases by about a factor of two. Moreover, the $N(OVII)$ distributions display tails towards significantly larger values with a few lines-of-sight exceeding the Yao et al. (2008) limit — this highlights the importance of excluding “contamination” from the disc and

Figure 4. Logarithm of $N(OVII)$ in cm^{-2} for the three simulated galaxies, excluding the disc, satellites or HVCs. From top to bottom: K33, K26, K15

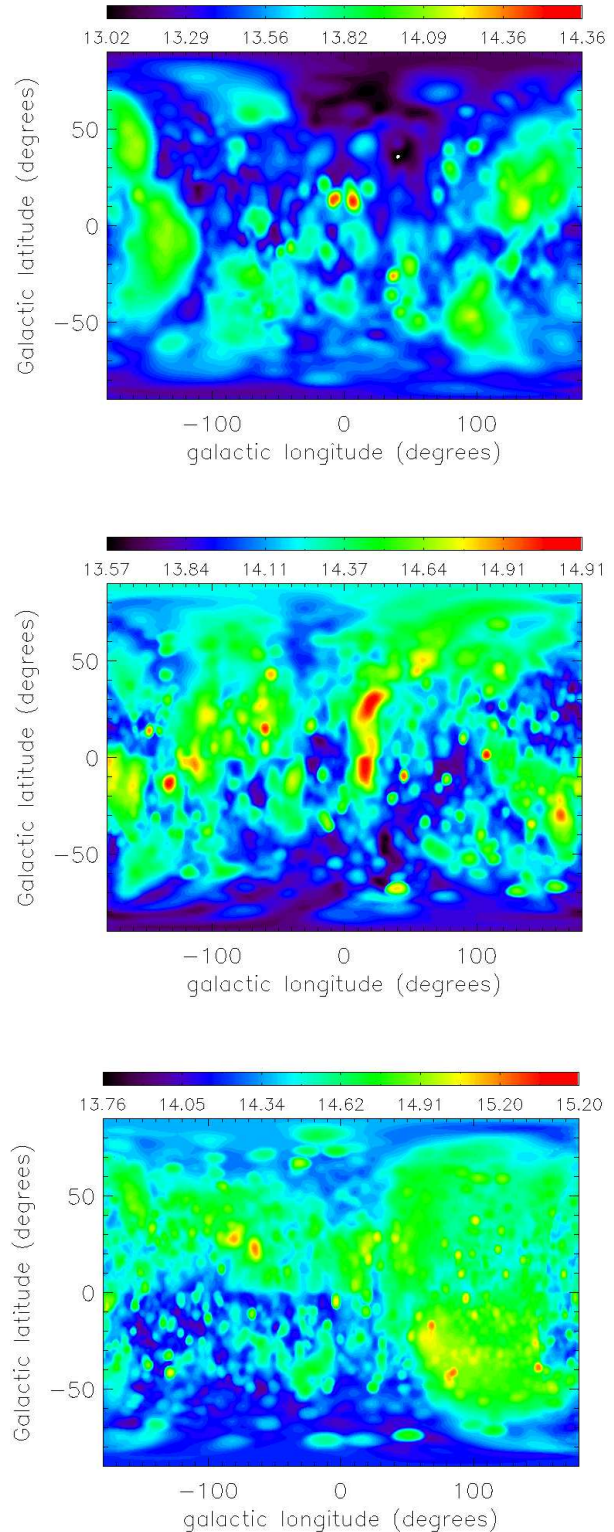


Figure 2. Histograms of the number of lines of sight at each column density bin. Left column: Blue dashed histograms result from including all gas particles, while red solid histograms result from excluding the disc and "dense" halo objects (see text for details). Right column: Red solid histograms are the same as shown in the right column (including a UV background and excluding the disc and "dense" halo objects), blue dashed histograms result from excluding the UV background (see text for details). Numbers are normalized to the total number of lines for each model. From top to bottom: K33, K26, K15

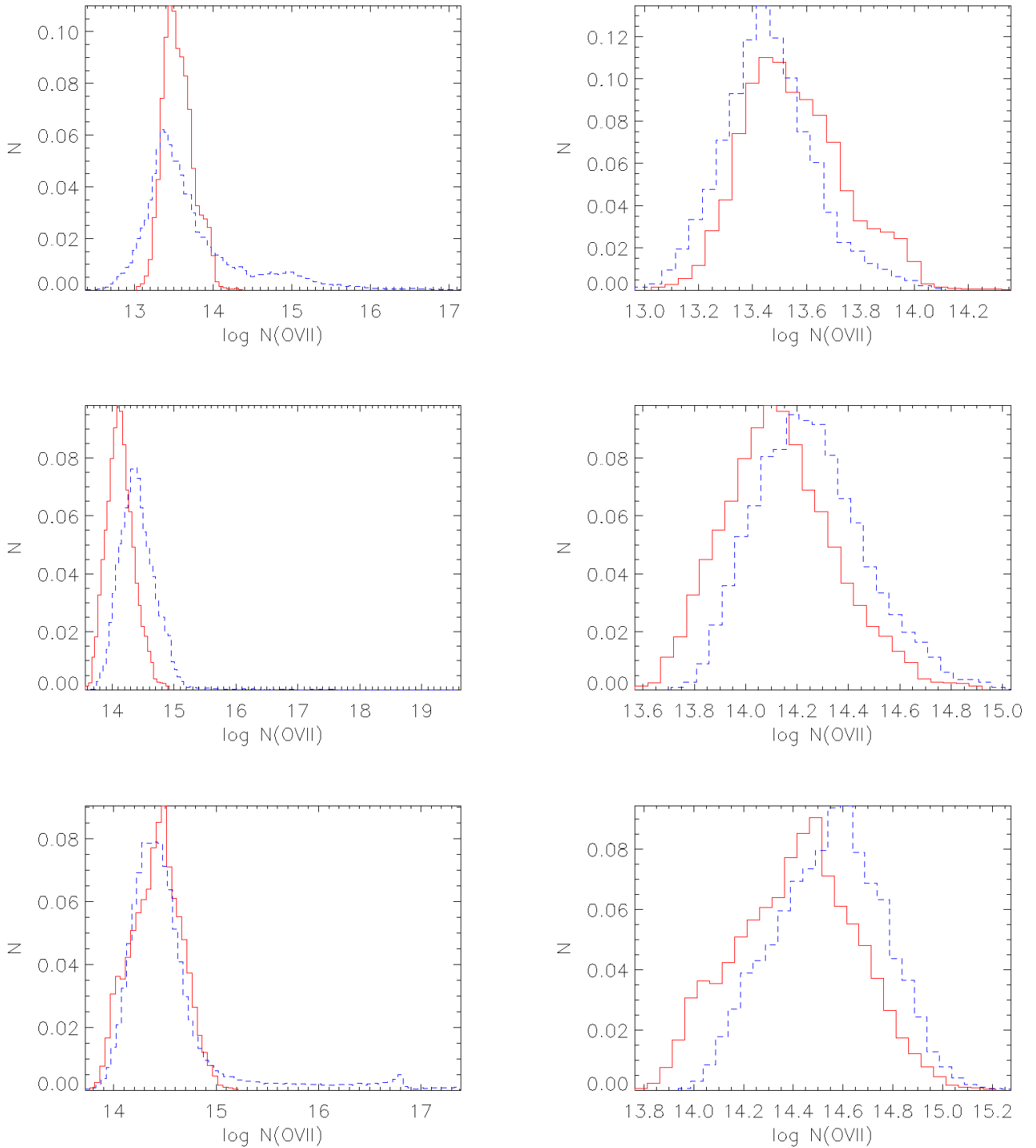


Figure 3. Cumulative histograms of the O VII column densities (fraction of lines of sight with column densities smaller than the corresponding column density bin). Left column: Blue dashed histograms result from including all gas particles, while red solid histograms result from excluding the disc and "dense" halo objects (see text for details). Right column: Red solid histograms are the same as shown in the right column (including a UV background and excluding the disc and "dense" halo objects), blue dashed histograms result from excluding the UV background (see text for details). From top to bottom: K33, K26, K15

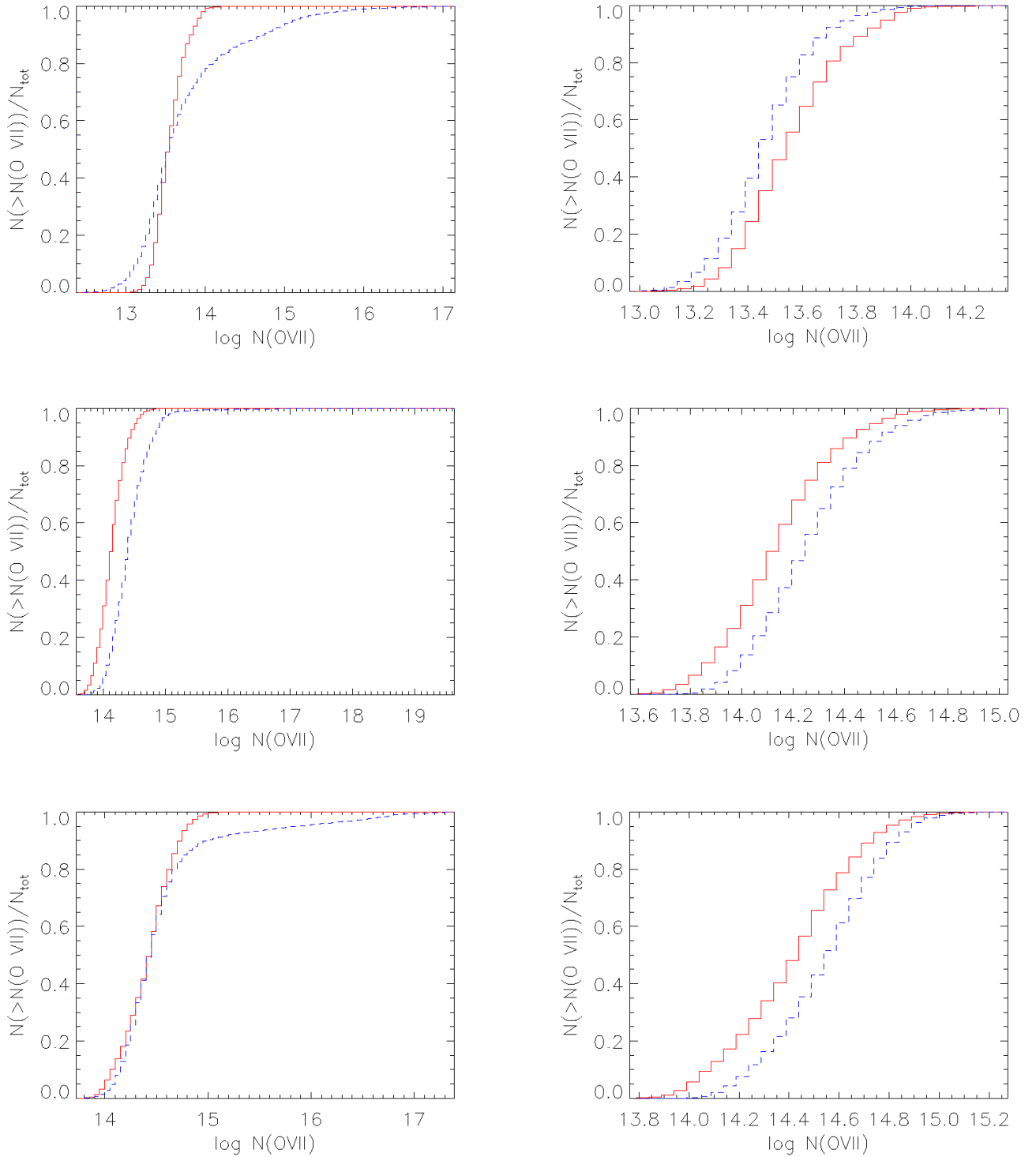


Figure 5. Logarithm of $N(\text{O VII})$ in cm^{-2} for the three simulated galaxies, including the disc and all objects in the halo. From top to bottom: K33, K26, K15

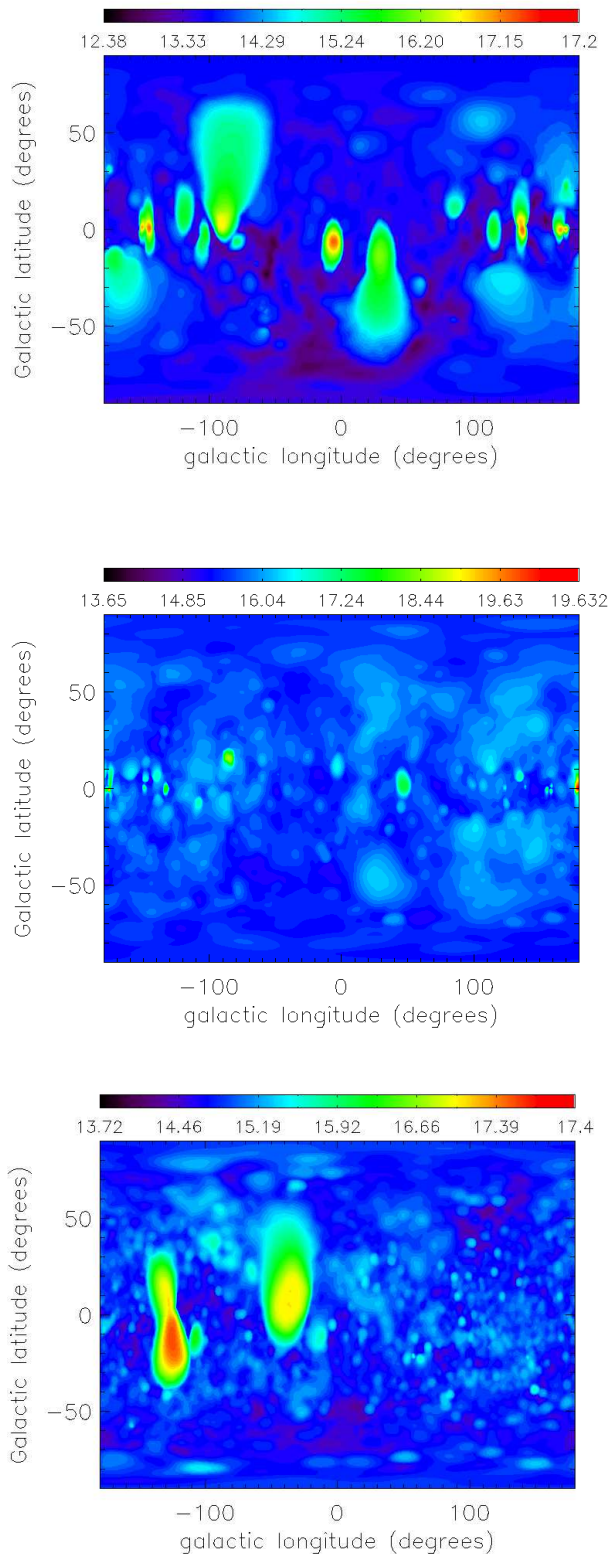
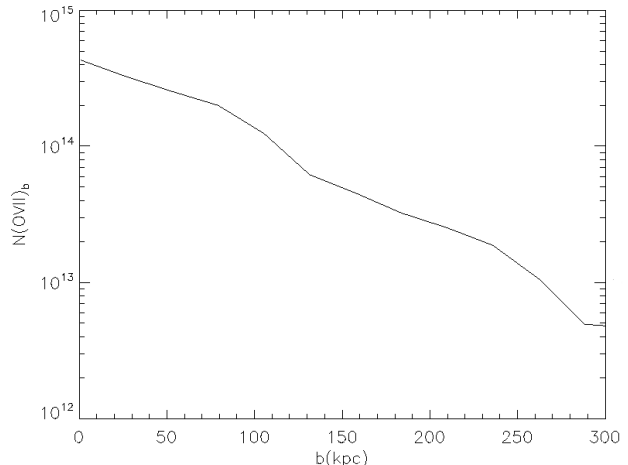


Figure 6. $N(\text{O VII})$ as a function of the impact parameter b for galaxy K15, which has a characteristic circular speed similar to that of M31.



other non-halo components, as discussed by the same authors. It also strongly suggests that the routinely reported ionic column densities of $N(\text{O VII}) \sim 10^{16} \text{cm}^{-2}$ at zero redshift originate in gas located near or inside the galactic disc, while the extended gaseous corona has a much lower contribution. The largest values of $N(\text{O VII})$ along a few lines-of-sight are mainly caused by either hot, super-nova driven bubbles in the disc gas or (in the case of K33) an outer, partly photo-ionized warp, originating from gas stripped off a previously accreted satellite.

To test the sensitivity of our results on the assumed UVB and (simplified) radiative transfer scheme, we repeated the calculations assuming no UVB. For the two Milky Way like galaxies, this leads to marginally larger median $N(\text{O VII})$ values. The reason for this is that at the (virial) temperatures of the halo gas, O VII is the most abundant oxygen state, and with the UVB switched on, some of the O VII ions are photo-ionized to (mainly) the O VIII stage, lowering the population of O VII ions. For the lower mass galaxy K33, on the other hand, the effect of the UVB is to boost the O VII ion population. This is confirmed by calculations (not presented in this paper) of the O VI and O VIII column densities for the same lines of sight.

Finally, we have tried to quantify the effect a neighbouring galactic halo might have on the O VII column density for a random line of sight. The probability of that happening and the relative effect this might have on the final result depends, of course, on the sizes of the two galaxies and on the distance between them. In a simple calculation, we have randomly chosen the starting and ending coordinates of 10000 lines of sight outside a certain halo and calculated their O VII column densities. We find that the contribution is very small unless the impact parameter of the line of sight to the centre of the galaxy is lower than 100-200kpc. Including the disc gas and satellites in this case does not alter the results presented above unless the impact parameter is very small (smaller than 50kpc). This is in agreement with what [Bregman & Lloyd-Davies \(2007\)](#) find for their line of sight

passing closest to M31, at a distance of 380kpc, giving no substantial contribution to the absorption.

Considering this result, possible contamination to the lines of sight that probe the Milky Way halo could likely only come from M31 (more distant galaxies would have their O VII line redshifted, so it would be relatively easy to distinguish their halo gas contribution from the one coming from local gas; this is beyond the scope of this paper, and will be the topic of a forthcoming paper — see also below). M31 is located at a distance of approximately 700kpc from our galaxy, which would cause it to contribute to the O VII column density with more than 10^{14}cm^{-2} for only about 0.5% of the sky area ($b \lesssim 100\text{kpc}$ — see Fig. 6). Excluding $b \leq 200\text{kpc}$ would reduce the M31 contribution to less than about $2 \times 10^{13}\text{cm}^{-2}$, and still only exclude about 2% of the sky area.

As mentioned above, it will be the topic of a forthcoming paper to investigate the contribution from the haloes of other, more distant galaxies. This study will be based on the proper statistical descriptors at the large-scale galaxy distribution.

In conclusion, the present observational upper limit is perfectly consistent with the results of state-of-the-art galaxy formation models, based on fully cosmological simulations. Moreover, although the predicted halo $N(\text{O VII})$ values lie below the observational upper limit, the difference is still only about an order of magnitude. With more sensitive future X-ray observatories, such as IXO, which will provide an order of magnitude increase in collecting area and a very high spectral resolution, it is very likely that one will be able detect O VII in the halo of the Milky Way, and possibly also in the haloes of other galaxies.

ACKNOWLEDGMENTS

We gratefully acknowledge abundant access to the computing facilities provided by the Danish Centre for Scientific Computing (DCSC). This work was supported by the DFG Cluster of Excellence “Origin and Structure of the Universe”. The Dark Cosmology Centre is funded by the Danish National Research Foundation.

REFERENCES

- Asplund M., Grevesse N., Sauval A. J., 2005, in Barnes III T. G., Bash F. N., eds, *Cosmic Abundances as Records of Stellar Evolution and Nucleosynthesis* Vol. 336 of *Astronomical Society of the Pacific Conference Series*, The Solar Chemical Composition. pp 25–+
- Bregman J. N., Lloyd-Davies E. J., 2007, *ApJ*, 669, 990
- Brüns C., Kerp J., Kalberla P., Mebold U., 2000, *A&AS*, 357, 120
- Fang T., Mckee C. F., Canizares C. R., Wolfire M., 2006, *ApJ*, 644, 174
- Ferland G. J., Korista K., Verner D., Ferguson J., Kingdon J., Verner E., 1998, *PASP*, 110, 761
- Ganguly R., Sembach K. R., Tripp T. M., Savage B. D., 2005, *ApJS*, 157, 251
- Greevich J., Putman M., 2009, *ApJ*, 696, 385
- Haardt F., Madau P., 1996, *ApJ*, 461, 20
- Haardt F., Madau P., 1997, in Wickramasinghe D. T., Bicknell G. V., Ferrario L., eds, *IAU Colloq. 163: Accretion Phenomena and Related Outflows* Vol. 121 of *Astronomical Society of the Pacific Conference Series*, *The Intrinsic UV/Soft X-Ray Spectrum Of Quasars*. pp 711–+
- Mastropietro C., 2009, in *The Magellanic System: Stars, Gas, and Galaxies* Vol. 256 of *Proceedings of the International Astronomical Union, IAU Symposium*, Modeling a high velocity LMC: The formation of the Magellanic Stream. pp 117–+
- Nicastro F., Mathur S., Elvis M., Drake J., Fang T., Fruscione A., Krongold Y., Marshall H., Williams R., Zezas A., 2005, *Nat*, 433, L495
- Nicastro F., Zezas A., Drake J., Elvis M., Fiore F., Fruscione A., Marengo M., Mathur S., Bianchi S., 2002, *ApJ*, 573, 157
- Peek J., Putman M., Sommer-Larsen J., 2008, *ApJ*, 674, 227
- Rasmussen A., Kahn S. M., Paerels F., den Herder J., de Vries C., 2003, in *Bulletin of the American Astronomical Society* Vol. 35 of *Bulletin of the American Astronomical Society*, *Observational limits to highly ionized absorption systems in the intergalactic medium for $z \leq 0.15$* . pp 605–+
- Rasmussen J., Sommer-Larsen J., Pedersen K., Toft S., Benson A., Bower R. G., Grove L. F., 2009, *ArXiv e-prints*
- Saha M. N., 1921, *Royal Society of London Proceedings Series A*, 99, 135
- Sembach K. R., Wakker B. P., Savage B. D., Richter P., Meade M., Shull J. M., Jenkins E. B., Sonneborn G., Moos H. W., 2003, *ApJS*, 146, 165
- Shull J., Jones J., Danforth C., Collins J., 2009, *ApJ*, 700, in press
- Sommer-Larsen J., 2006, *ApJL*, 644, 1
- Sommer-Larsen J., Götz M., Portinari L., 2003, *ApJ*, 596, 47
- Springel V., Hernquist L., 2002, *MNRAS*, 649, 649
- Stanimirović S., Hoffman S., Heiles C., Douglas K. A., Putman M., Peek J. E. G., 2008, *ApJ*, 680, 276
- Toft S., Rasmussen J., Sommer-Larsen J., Pedersen K., 2002, *MNRAS*, 335, 799
- Wakker B. P., Savage B. D., Sembach K. R., Richter P., Fox A. J., 2005, in Braun R., ed., *Extra-Planar Gas* Vol. 331 of *Astronomical Society of the Pacific Conference Series*, *High-velocity O VI in and near the Milky Way*. pp 11–+
- Yao Y., Nowak M., Wang Q., Schulz N., Canizares C., 2008, *ApJ*, 672, L21
- Yao Y., Wang Q. D., Penton S. V., Tripp T. M., Shull J. M., Stocke J. T., 2010, *ApJ*, 716, 1514